

Ceramic materials prepared from nanocrystalline InFeZnO₄ powder: optical and mechanical properties, and evaluation of radiation tolerance

Olga N. Kondrat'eva^{1,a}, Maria N. Smirnova^{1,b}, Galina E. Nikiforova^{1,c},
Alexey D. Yapryntsev^{1,d}, Dmitriy F. Kondakov^{1,e}, Leonid D. Yagudin^{2,f}

¹Kurnakov Institute of General and Inorganic Chemistry of the Russian Academy of Sciences, Moscow, 119991, Russia

²Frumkin Institute of Physical Chemistry and Electrochemistry of the Russian Academy of Sciences, Moscow, 119071, Russia

^aol.kondratieva@gmail.com, ^bsmirnovamn@igic.ras.ru, ^cgen@igic.ras.ru,

^dyapryntsev@igic.ras.ru, ^eoldradio@mail.ru, ^fyagudinld@icloud.com

Corresponding author: O. N. Kondrat'eva, ol.kondratieva@gmail.com

PACS 81.07.Wx, 62.20.Qp, 78.20.-e

ABSTRACT A method for low-temperature synthesis of InFeZnO₄ oxide from an X-ray amorphous precursor formed as a result of the thermal decomposition of dehydration product of a mixture of polyvinyl alcohol and iron, indium, and zinc nitrate solutions has been developed. Using TG/DSC and XRD, the InFeZnO₄ phase has been shown to be formed in the temperature range of 370–420°C. Using the XRD method, after the heat treatment of the precursor at 800°C for 4 hours, nanocrystalline InFeZnO₄ with an average particle size (CSR) of ≈36 nm has been found to be formed. According to SEM, they do not have a clear facet and form a homogeneous cellular microstructure of the powder. The absence of organic residues and moisture in it has been confirmed by FTIR spectroscopy. From the DRS data, it has been found that the band gap energy E_g of InFeZnO₄ for the cases of indirect and direct transitions is 1.54 eV and 2.25 eV, respectively. Ceramics produced from nanocrystalline InFeZnO₄ by high-temperature sintering have a density equal to 5160 kg/m³ (≈86 % of the theoretical one). Their microhardness, measured by the Vickers method, is 2.12 GPa. The radiation resistance of InFeZnO₄ has been predicted, from which it follows that, when exposed to intermediate and high doses of ionizing radiation, its partial amorphization is the most likely.

KEYWORDS Indium-iron-zinc oxide; rhombohedral crystal structure; X-ray amorphous precursor; nanoscale powders; sintering; ceramics; microhardness; band gap energy; radiation tolerance.

FUNDING This study was performed within the ARIADNA Collaboration operating under the NICA facility as a part of State Assignment of the IGIC RAS “Solving topical problems with NICA charged particle beams” (ref. # 1024050300012-6-1.4.2).

ACKNOWLEDGEMENTS The measurements were performed using the equipment of the JRC PMR IGIC RAS. The microhardness studies were carried out using the equipment of the CKP FMI IPCE RAS.

FOR CITATION Kondrat'eva O.N., Smirnova M.N., Nikiforova G.E., Yapryntsev A.D., Kondakov D.F., Yagudin L.D. Ceramic materials prepared from nanocrystalline InFeZnO₄ powder: optical and mechanical properties, and evaluation of radiation tolerance. *Nanosystems: Phys. Chem. Math.*, 2024, **15** (5), 693–701.

1. Introduction

The development of new, technologically simple and economically advantageous methods for the production of highly dispersed oxides RMO₃(M'O)_m (where R = Sc, In, Y, or Er–Lu; M = Fe, Ga, or Al; M' = Zn; m = 1, 2, 3 ...), combining high thermal stability and potentially promising functional properties are of great interest both from a fundamental and practical point of view [1–5]. For example, materials based on InGaO₃(ZnO)_m (m = 1–4), owing to their unique electro- and thermophysical characteristics, have already been applied as components of displays and sensor devices [6–8]. A number of complex iron, indium, and zinc oxides InFeO₃(ZnO)_m (where m = 1–19) belong to refractory oxides that have been relatively poorly studied. In particular, Kimizuka et al. established [9] that some of these oxides (m = 1, 2, 3, 7, 9, 11, 13, 15 and 19) remain thermally stable when heated up to 1550°C, and continuous exposure to very high temperatures (7 days at 1250°C) does not cause changes in their phase and/or chemical composition. The results of the thermophysical characteristics of ceramic materials InFeO₃(ZnO)_m (m = 1–5) showed [10] that InFeZnO₄ oxide has the lowest thermal conductivity in this series (≈ 2.8 W/(m·K) at 25°C). Its value is closely equal to the thermal conductivity of thermal barrier materials that are already in use, such as 7-8 wt. % yttria-stabilized zirconium dioxide

(YSZ) ($\approx 3.0 \text{ W/(m}\cdot\text{K)}$ at 25°C [11]). The low thermal conductivity of InFeZnO_4 oxide in combination with a thermal expansion coefficient ($11.7 \times 10^{-6} \text{ K}^{-1}$ [12]), close in magnitude to YSZ ($10.7 \times 10^{-6} \text{ K}^{-1}$ [13]), makes it potentially suitable for creating special thermal barrier coatings used on the surface of structural materials from which parts and nodes of aerospace equipment are produced [12, 14–16]. Moreover, it is noted in [10] that the relatively low hardness and low friction coefficient make InFeZnO_4 promising in terms of creating abrasible seal coating materials with high thermal insulation. Doping or the introduction of an additional phase into the material [10, 14, 16] as well as the use of nanoscale precursors for its production can be considered as a strategy to improve the functional characteristics of InFeZnO_4 . On the other hand, it is possible to change (and even significantly improve) the performance of a material by exposing it to high pressures or various doses of high-energy ion irradiation. For example, in [17] it is noted that irradiation of magnesium aluminate with Mg^+ ions with an energy of 2.4 MeV and a fluence of 1.4×10^{21} ions/cm² results in an increase in its hardness compared with a non-irradiated sample by 5%, and when irradiated with high doses of neutrons [18] it leads to a noticeable decrease in thermal conductivity.

To date, the general method of obtaining InFeZnO_4 ceramic materials is that of solid-phase interaction. Analysis of literature data [9, 10, 12, 19, 20] showed that a mechanical mixture of In_2O_3 , Fe_2O_3 and ZnO oxides which is subjected to prolonged (up to 5 days) multistage annealing at temperatures in the range of $1300\text{--}1550^\circ\text{C}$ is used to produce it. Furthermore, it is reported in some works that InFeZnO_4 synthesized in such a way contains an admixture of $\text{InFeO}_3(\text{ZnO})_2$ [12] or ZnFe_2O_4 [20]. In particular, an approach as an alternative, energy-efficient method for the production of InFeZnO_4 can be used. It includes the stages of obtaining a composition consisting of a polymer (polyvinyl alcohol (PVA), starch, etc.) and aqueous mixtures of nitrates of the corresponding metals, its thermal decomposition, and subsequent annealing of the resulting X-ray amorphous precursor at relatively low temperatures. It was shown in [21, 22] that using this approach, it is possible to synthesize single-phase, nano- and microcrystalline powders of various complex metal oxides at temperatures of $800\text{--}1000^\circ\text{C}$.

This paper presents for the first time the development results of the low-temperature synthesis basics of InFeZnO_4 oxide from a PVA-nitrate composition, and discusses the structural and physical and mechanical characteristics of a ceramic material made on its basis. Taking into account the potential applications of the material in question, the prediction results of radiation-induced changes occurring in its crystal structure at intermediate and high doses of ionizing radiation are also presented. These data may be of interest in determining the limits of applicability of InFeZnO_4 ceramic materials when operated under radiation conditions, and also when their properties are directionally changed by exposure to various doses of ionizing radiation.

2. Experimental part

2.1. Synthesis of InFeZnO_4 powder

The point of the synthesis method of InFeZnO_4 oxide was to prepare a composition containing a polymer and nitrate solutions of the corresponding metals, its evaporation and thermal decomposition, and subsequent annealing of the resulting solid-phase product. Polyvinyl alcohol ($(\text{CH}_2\text{CHOH})_n$, GOST 10779-78) and aqueous solutions of indium, iron, and zinc nitrates were used as initial reagents. Their quantity was calculated using the reaction equation given below:



To prepare aqueous solutions of metal nitrates, nitric acid (high purity grade, 18-4, GOST 11125-84), zinc (grade Z0, $\omega(\text{Zn}) = 99.975 \text{ wt. \%}$, GOST 3640-94), indium (grade In0, $\omega(\text{In}) = 99.998 \text{ wt. \%}$, GOST 10297-94) and carbonyl iron (high purity grade, 13-2, TS 6-09-05808009-262-92) were used. The metals were dissolved in acid previously diluted with distilled water in a ratio of 1 : 3 by volume. Solutions $\text{In}(\text{NO}_3)_3$, $\text{Fe}(\text{NO}_3)_3$ and $\text{Zn}(\text{NO}_3)_2$ were mixed and then concentrated on a heating plate at 90°C . Evaporating a mixture of salt solutions, PVA was added with constant stirring. The resulting gel-like mass (hereinafter referred to as the gel) was continued to be heated on a plate until a voluminous brown powder was obtained. The resulting powder was thoroughly ground and then annealed at temperatures ranging from 600°C to 1200°C . The heat treatment was carried out in air, and its duration at each temperature was at least 4 hours.

2.2. Production of InFeZnO_4 ceramics

Nanocrystalline powder InFeZnO_4 was used to produce dense ceramics. A few drops of acetone were added to it and carefully ground in an agate mortar. Cylindrical samples with a height of $\approx 5 \text{ mm}$ and a diameter of $\approx 14 \text{ mm}$ were formed from the produced mass by cold uniaxial pressing. Sintering of the samples was carried out in air at 1350°C for 4 hours. The density of ceramics after sintering was estimated by its geometric dimensions and mass. The relative density was expressed as a percentage of the XRD density.

2.3. Thermal analysis

Thermogravimetry and differential scanning calorimetry (TG/DSC) were used to study the processes occurring during gel heating and to establish the temperature range in which the formation of the crystalline phase of InFeZnO_4 occurred. The measurements were carried out on a MOM Derivatograph Q-1500D with an upgraded heater control unit and a

registration system. A gel sample weighing 0.1500 g was heated in a platinum crucible in the temperature range of 25–1000°C with a heating rate of 10°C/min. The sensitivity of thermobalance was 200 mg, and its accuracy was $\pm 0.5\%$. The temperature measurement error did not exceed $\pm 3^\circ\text{C}$.

2.4. Phase composition, microstructure and mechanical properties

The structure and phase composition of the synthesized materials before and after their heat treatment were studied using powder X-ray diffraction (XRD). XRD patterns were recorded at ambient temperature on a Bruker D8 Advance powder diffractometer (X-ray tube with copper anode $\lambda(\text{CuK}\alpha) = 1.5418 \text{ \AA}$) equipped with a LynxEye linear detector and a nickel filter. The measurement results were processed using Bruker DIFFRAC.EVA software. Crystal phases were identified using the electronic diffraction database ICDD PDF-2. Scanning electron microscopy (SEM) was used to determine the structural and morphological characteristics of synthesized materials. SEM images were obtained using an ultra-high resolution scanning electron microscope TESCAN AMBER. The ceramics were tested for microhardness using the Vickers method on a LOMO PMT-3M device. The samples were pre-polished and washed in an aqueous alcohol solution under ultrasound. The measurements were carried out at a load of 0.98 N (100 g), the duration of exposure under load was 10 seconds.

2.5. Optical and spectral properties

The change in the moisture content and carbon-containing impurities in the powders with an increase in annealing temperature was controlled using Fourier-transform infrared spectroscopy (FTIR). A Perkin Elmer Spectrum 65 FT-IR spectrometer was used to register FTIR spectra in the 400–4000 cm^{-1} region.

Diffuse reflectance spectroscopy (DRS) data were used to determine the band gap energy E_g of InFeZnO_4 oxide. Diffuse reflectance spectra (R) were obtained using the Ocean Optics modular optical system (QE65000 detector, HPX-2000 xenon source, integrating sphere ISP-80-8-R with a diameter of 80 mm). Measurements were carried out in the wavelength range from 200 to 1000 nm. The Ocean Optics WS-1 standard from polytetrafluoroethylene was used as a reference sample. The E_g value was calculated using the Tauc plot in coordinates $(F(R) \cdot h\nu)^n - h\nu$, where $F(R)$ is the Kubelka–Munk function equal to $(1-R)^2/2R$, h is Planck's constant, ν is the frequency of incident radiation, n is a constant characterizing the type of transition ($n = 1/2$ and $n = 2$ correspond to indirect and direct transitions, respectively).

3. Results and Discussion

3.1. Results of XRD and FTIR studies of synthesized powders

Fig. 1(a) demonstrates XRD patterns of powders before (profile 1) and after (profiles 2–4) solid-phase product annealing formed as a result of heating and thermal decomposition of an initial reagent mixture. A blurred halo can be noted on the XRD pattern of the unannealed sample (profile 1), observed in the existence region of the main diffraction lines of InFeZnO_4 oxide ($2\theta \approx 28\text{--}38^\circ$). Furthermore, the absence of any diffraction maxima indicates the X-ray amorphous nature of the powder in question. Its FTIR spectrum is shown in Fig. 1(b) (spectrum 1). The absorption bands observed in the region of 1600–1700 cm^{-1} can be attributed to deformation vibrations of the –OH bonds of water molecules, while the wide band at 3355 cm^{-1} can be attributed to valence ones [23]. The presence of these bands in the FTIR spectrum of the X-ray amorphous powder allows us to conclude that there is sorption of water vapor on the surface of its particles. The bands located in the region of 1450–1300 cm^{-1} and at 800 cm^{-1} are related to stretching vibrations of N–O bonds and bending vibrations of the NO_3^- group [23–25]. From the FTIR spectrum of the sample annealed at a temperature of 600°C, the intensity of the absorption bands connected with the presence of moisture and organic impurities can be seen to decrease markedly. In addition, wide diffraction peaks appear on the XRD pattern of this powder (Fig. 1(a), profile 2), indicating a high degree of dispersion and imperfection in the crystalline structure of the formed phase.

An increase in the annealing temperature to 800°C leads to that in the intensity of diffraction maxima relating to the InFeZnO_4 phase (Fig. 1(a), profile 3). Moreover, intense absorption bands (478 cm^{-1} and 532 cm^{-1}) appear on the FTIR spectrum of this powder due to vibrations of metal–oxygen bonds. The bands observed above 1000 cm^{-1} (Fig. 1(b), spectrum 3) disappear completely, indicating dehydration of the sample and the absence of carbon-containing residues in it. Fig. 1(b) (spectrum 4) shows that powder annealing at 1000°C has almost no effect on the shape and position of the bands in the FTIR spectrum. In addition, the diffraction maxima become narrower and more intense (Fig. 1(a), profile 4), which indicates the continuous ordering and improvement of the InFeZnO_4 crystal structure.

3.2. Thermal behavior of the gel

In order to establish the temperature range in which the formation of the crystalline phase of InFeZnO_4 occurs, the features of thermal decomposition of the gel prepared by evaporation of an initial reagent mixture are investigated. The results of TG and DSC of the test sample in the range of 25–1000°C are shown in Fig. 2(a,b). Analysis of the thermogram and its first derivative in temperature (DTG) (Fig. 2(a)) shows that the thermal decomposition of the gel occurs in several stages. At the first stage which is observed in the range of 60–267°C, the test sample loses almost half of its mass (46.82%). This process is accompanied by a complex endothermic effect (63–234°C) with a minimum at 144°C (Fig. 2(b)). The significant mass loss appears to have been caused by the removal of moisture, nitrogen oxides, and gaseous

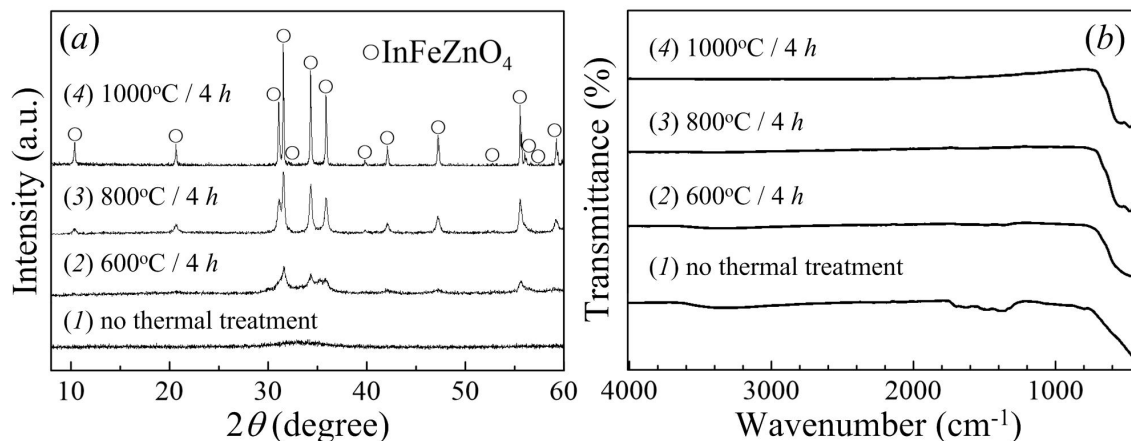


FIG. 1. (a) XRD patterns and (b) FTIR spectra of powders obtained after annealing of a precursor formed as a result of thermal decomposition of the dehydration product of an initial reagent mixture

organic compounds produced as a result of the destruction of organo-inorganic products formed after dehydration of the initial reagent mixture. When there is a further increase in temperature, a less intense exothermic effect appears on the DSC curve ($\approx 370\text{--}420^\circ\text{C}$), having a maximum at 392°C . The mass loss corresponding to this effect occurs in the range of $267\text{--}430^\circ\text{C}$ and is 18.22%. It can be assumed to be related to the continued removal of gaseous decomposition products. Ultrafine particles of InFeZnO_4 begin to form at 370°C alongside with this process. This is supported by the absence of thermal effects above 430°C (Fig. 2(b)) and the results of XRD (Fig. 1(a), profile 2), according to which oxide particles with a CSR size of $\approx 15\text{ nm}$ are formed at temperatures below 600°C . A slight mass loss (2.56%) which completes at a temperature of $\approx 778^\circ\text{C}$ (Fig. 2(a)) is connected with the final removal of carbonaceous residues and surface-adsorbed water, which is confirmed by the results of FTIR spectroscopy (Fig. 1(b), profile 3).

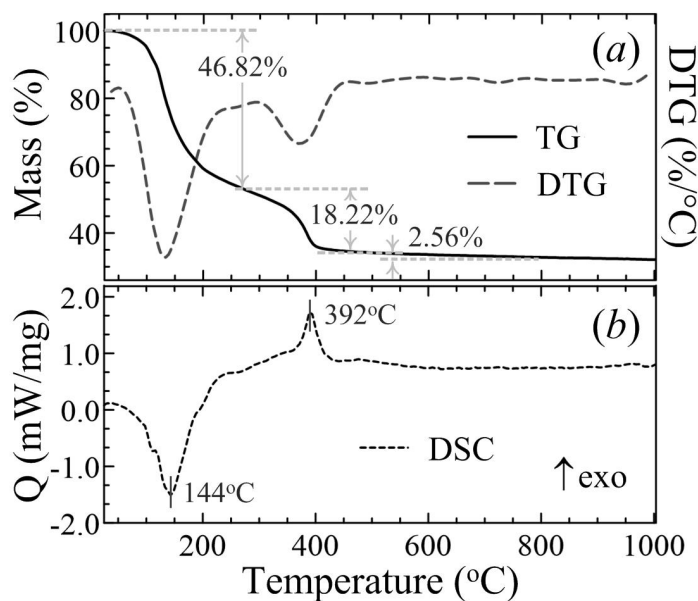


FIG. 2. (a) TG/DTG and (b) DSC curves of the gel

3.3. Microstructural characteristics of InFeZnO_4 powder

SEM images showing the change in the InFeZnO_4 powder microstructure with an increase in the annealing temperature from 800°C to 1200°C are shown in Fig. 3 (a–c). They show that the powder annealed at 800°C for 4 hours (Fig. 3(a)) has a cellular microstructure formed by very small grains without an apparent crystalline cut, which is consistent with XRD data. The average size of the crystalline grain of the InFeZnO_4 phase, which is assumed to be equal to the average size of the CSR, is 36 nm. When the annealing temperature rises to 1000°C , it increases to $\approx 90\text{ nm}$. This correlates with the SEM data (Fig. 3(b)) showing that the grain size of InFeZnO_4 is noticeably enlarged. An increase in the annealing temperature to 1200°C leads to the production of a microcrystalline powder consisting of well-faceted InFeZnO_4 grains

with a size of 2–5 μm (Fig. 3(c)). The XRD pattern of this powder is shown in Fig. 3(d). Its analysis demonstrates that all observed diffraction maxima relate to InFeZnO_4 . The parameters of its unit cell (s.g. R-3m; Z = 3) are: $a = 3.3194(1)$ \AA ; $c = 26.1310(4)$ \AA ; $V = 249.35(1)$ \AA^3 ; $\rho_{XRD} = 5998$ kg/m^3 . Thus, the results of XRD and SEM reveal that an increase in the annealing temperature of the X-ray amorphous powder (Fig. 1(a), profile 1) does not lead to the appearance of secondary phases and is accompanied only by the enlargement of the InFeZnO_4 grains and the improvement of their crystalline faceting.

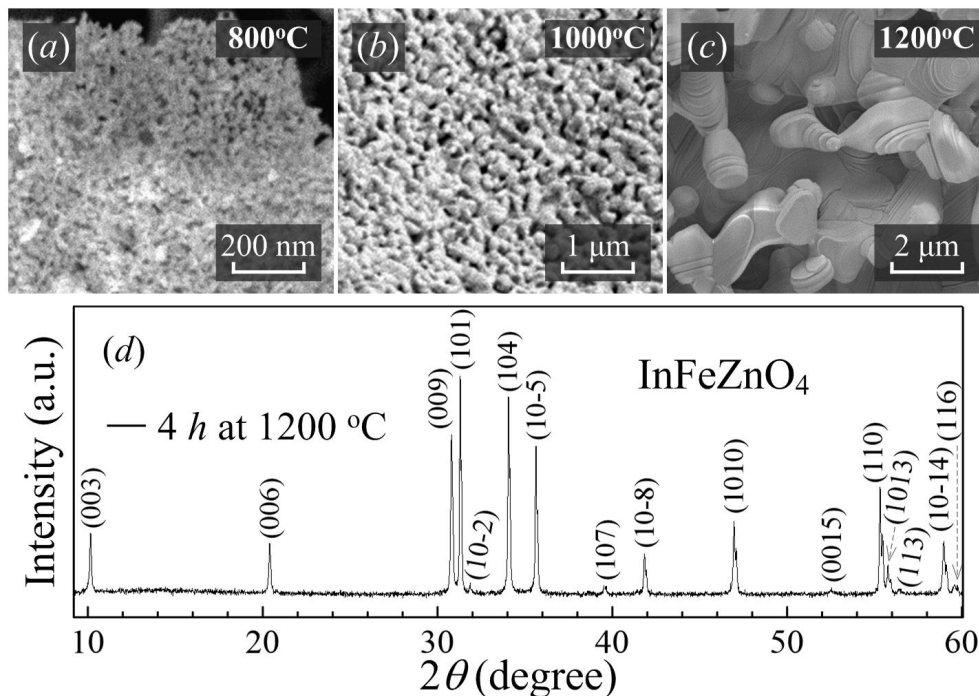


FIG. 3. (a-c) SEM images of InFeZnO_4 powder annealed at temperatures of 800°C, 1000°C and 1200°C for 4 hours in air. (d) XRD pattern of the powder annealed at a temperature of 1200°C

3.4. Structure and mechanical properties of InFeZnO_4 ceramics

It is preferable to use powders with particle sizes varying within a few tens of nanometers for the manufacture of fine-grained and non-porous ceramics. In this regard, a nanocrystalline powder annealed at a temperature of 800°C is used to produce a dense and structurally homogeneous sample of InFeZnO_4 ceramics. A typical image of the ceramics obtained from this powder is shown in Fig. 4(a). It has a uniform dark brown staining, and its surface has no cracks after sintering. SEM images of the cleavage of InFeZnO_4 ceramics at different magnifications are shown in Fig. 4(b,c). The SEM examination also revealed no cracks (Fig. 4(b)), which indicates the correctness of the parameters chosen for the manufacture of ceramics. Fig. 4(c) clearly shows that the ceramic structure is formed by large (up to several tens of micrometers) grains with a layered structure. It can also be noted that single small pores with a diameter of 1–2 microns are visible on the surface of the cleavage, which indicates a quite high density of ceramics. Its density, which is found using the geometric method, is 5160 kg/m^3 , which is $\approx 86\%$ of the theoretically possible one.

The analysis has shown that there are no data on Vickers microhardness for InFeZnO_4 and related oxides in the literature so far. According to the results of testing InFeZnO_4 ceramics for microhardness using the Vickers method, the average value of its microhardness number is found to be 216.3 ± 35.0 (2.12 ± 0.34 GPa). To evaluate the hardness class of InFeZnO_4 , the ratio proposed by Khrushchev [26] was used (Eq. (1)):

$$H_0 = 0.675 \times H^{1/3},$$

where H_0 is the hardness class on a 15–point scale, in which graphite corresponds to 1 and diamond to 15; H is the experimental value of the microhardness number, expressed in kgf/mm^2 . According to the results of calculation using Eq. (1), the hardness class of InFeZnO_4 ceramics on the Khrushchev scale is 4.1, which is comparable in magnitude to H_0 for such minerals as zincite and sphalerite (3.6–4.6) [27]. In terms of classification of minerals and synthetic materials by their hardness numbers [27], InFeZnO_4 can be attributed to materials of medium hardness (1.18–5.40 GPa).

3.5. Calculation of the band gap energy of InFeZnO_4

To date, the optical properties of InFeZnO_4 have not been extensively studied. Narendranath et al. [20] determined the band gap of this oxide from the DRS data under the assumption of an indirect transition ($E_g = 2.85$ eV). However, the

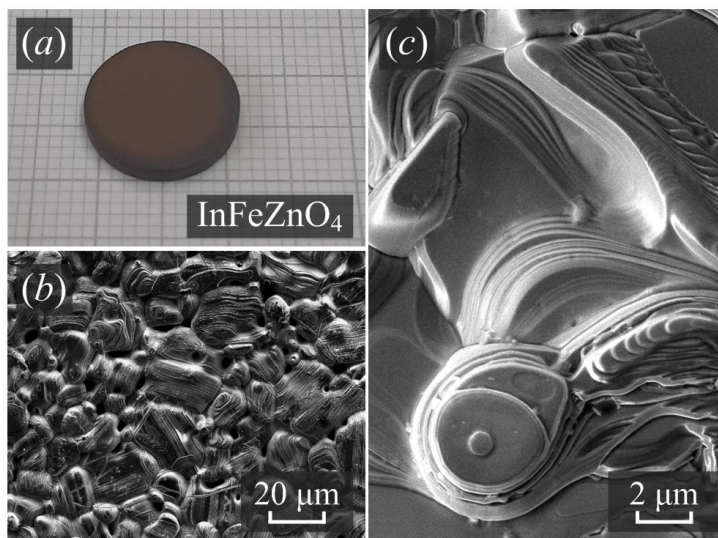


FIG. 4. (a) Digital image of InFeZnO_4 ceramics sintered at a temperature of 1350°C for 4 hours in air. (b, c) SEM images of the cleavage surface obtained at different magnifications

spectrum obtained by the authors contains many bands that can be attributed to both direct and indirect transitions [28]. On the other hand, when determining the E_g value of the isostructural oxides InGaZnO_4 [3] and InGaMgO_4 [29], the analysis was conducted under the assumption of direct transitions, though this choice was not discussed by the authors. Since there is no information about the type of optical transitions in InFeZnO_4 , the data that we obtained from the DRS (Fig. 5(a)) are presented in Tauc plot both under the assumption of direct and indirect transitions (Fig. 5(b)). For both cases, the band gap energy was found by extrapolating the linear section of the graph of the dependence $(F(R)\cdot h\nu)^n$ from $h\nu$ to the abscissa axis. The value of E_g InFeZnO_4 under the assumption of an indirect transition ($n = 1/2$) is 1.54 ± 0.01 eV, and for a direct transition ($n = 2$) it is 2.25 ± 0.01 eV. Both values obtained turn out to be noticeably lower compared to the previously published one in [20]. The reason for this discrepancy is not obvious, however, it can be assumed that the difference in E_g values is due to the fact that InFeZnO_4 samples obtained by different synthesis methods differ in their phase composition, as well as in the degree of dispersion and structural defects. The InFeZnO_4 sample obtained by solid-phase synthesis has a larger particle size compared to that synthesized in this work. Additionally, Narendranath et al. [20] note the presence of ZnFe_2O_4 impurity, which is not observed in our case.

3.6. Evaluation of InFeZnO_4 radiation resistance

Further, we will consider several criteria that allow us to draw a conclusion about the ability of the material to resist ionizing radiation. Structural changes occurring in a solid when exposed to intermediate ($\sim 10^{13} - 10^{16}$ ions/cm²) and high ($\geq 10^{17}$ ions/cm²) doses of high-energy ion irradiation can be reliably predicted using the criteria proposed by Naguib and Kelly [30]. The first of them is that the amorphization of a crystalline solid must occur if the ratio of its crystallization temperature (T_C) to the melting temperature (T_m) exceeds 0.30. The second criterion is based on the fact that the amorphization is most likely if the ionicity of the compound is $f \leq 0.47$. Moreover, compounds with f values in the range from 0.47 to 0.60 may be capable of both amorphization and preservation of their crystal structure under irradiation. The melting point of InFeZnO_4 is unknown, but the authors [9] established that this compound is thermally stable when heated to 1550°C . Therefore, in a rough approximation, this temperature can be assumed to be equal to the melting point. The temperature of the onset of crystallization of InFeZnO_4 , estimated from the DSC data (Fig. 2(b)), is approximately 370°C . The calculated value of the T_C/T_m ratio for the oxide studied is $\approx 0.33 > 0.30$, which indicates the possibility of its amorphization under irradiation. The ionicity of InFeZnO_4 is estimated by the Pauling equation using the electronegativity values of atoms from [31]. According to the calculation results, the ionicity is 0.528. The value obtained falls within the range between 0.47 and 0.60, which does not allow us to draw an unambiguous conclusion about the structural changes that can occur in InFeZnO_4 under irradiation. It can be noted that zinc ferrite ZnFe_2O_4 has the closest f value (0.535) to InFeZnO_4 . Satalkar et al. demonstrated [32] that as a result of irradiation of nanocrystalline ZnFe_2O_4 with $^{16}\text{O}^{6+}$ ions with an energy of 80 MeV and fluence up to 2×10^{14} ions/cm², only a slight increase in the volume of the unit cell (up to 0.64%) and a change in the degree of cationic disordering can be observed. The formation of other phases (crystalline or amorphous) has not been detected [32]. Furthermore, irradiation of a ceramic spinel sample with heavy Xe ions with an energy of the order of several GeV and a fluence of 6×10^{11} ions/cm² results in the formation of amorphous latent tracks [33]. Therefore, it can be concluded that their formation is expected in the case of InFeZnO_4 . Moreover, this oxide can also be assumed to have a higher radiation resistance in the nanocrystalline state. Taking into account the

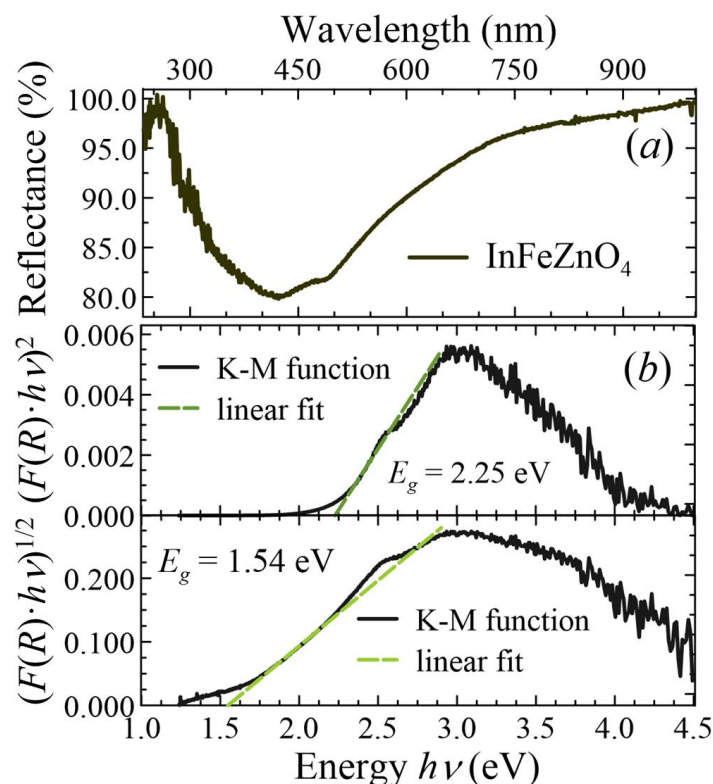


FIG. 5. (a) The diffuse reflectance spectrum of InFeZnO_4 and (b) its representation in Tauc coordinates for the case of indirect ($n = 1/2$) and direct ($n = 2$) transitions

promising thermophysical and mechanical properties of InFeZnO_4 , it can be summed up that nanoscale materials on its base may be suitable for use as radiation-resistant protective coatings with special thermal properties.

4. Conclusions

In this paper, the experimental results on the production of InFeZnO_4 oxide from an X-ray amorphous powder formed during the thermal decomposition of dehydration products of a PVA mixture and metal nitrate solutions are considered. The results of thermal analysis (TG/DSC) of the gel allow us to conclude that the ultrafine phase of InFeZnO_4 is formed in the range of 370–420°C. It is found by XRD that the solid decomposition products are in an X-ray amorphous state, and their annealing at temperatures of 600–800°C gives rise to the formation of a single-phase nanocrystalline powder InFeZnO_4 with a particle size of 15–36 nm. According to SEM data, the powder annealed at 800°C has a homogeneous, cellular microstructure formed by very small and poorly faceted grains, which correlates with the results of X-ray diffraction analysis. The absence of moisture and organic residues in it is confirmed by FTIR spectroscopy. InFeZnO_4 microcrystalline ceramic materials were produced using this powder. Their relative density after sintering at a temperature of 1350°C for 4 hours in air is 86% of the theoretical one. SEM studies have shown that a homogeneous and dense ceramic structure consisting of grains > 10 microns in size are obtained as a result of sintering. The microhardness of InFeZnO_4 ceramics, measured by the Vickers method, is 2.12 GPa. The result obtained makes it possible to classify the manufactured ceramics as materials with medium hardness. According to DRS data, it is revealed that the E_g value of InFeZnO_4 oxide, assuming indirect band transitions, is 1.54 eV, and for direct band transitions it is 2.25 eV. In order to predict structural changes that occur under ionizing radiation, criteria are also calculated, which allowed for the ionicity f of InFeZnO_4 and the ratio of its crystallization and melting temperatures (T_C/T_m). Analysis of the calculated values of f and T_C/T_m allows us to conclude that irradiation of this material with intermediate or high doses of high-energy ions is most likely to result in its partial amorphization. These preliminary conclusions can be taken into account while conducting experiments aimed at changing the functional properties of InFeZnO_4 by high-energy ion irradiation, as well as in the manufacture of coating materials and devices exposed to ionizing radiation, including cosmic radiation.

References

- [1] Kimizuka N., Takayama-Muromachi E., Siratori K. The systems $\text{R}_2\text{O}_3\text{--M}_2\text{O}_3\text{--M/O}$: R is In, Sc, Y or one of the lanthanides, M is Fe, Ga, or Al, and M' is one of the divalent cation elements. *Handbook on the Physics and Chemistry of Rare Earths*, 1990, **13**, P. 283–384.
- [2] Grajczyk R., Subramanian M.A. Structure–property relationships of YbFe_2O_4 - and $\text{Yb}_2\text{Fe}_3\text{O}_7$ -type layered oxides: A bird's eye view. *Progress in Solid State Chemistry*, 2015, **43**(1–2), P. 37–46.

- [3] Préaud S., Byl C., Brisset F., Berardan D. SPS-assisted synthesis of $\text{InGaO}_3(\text{ZnO})_m$ ceramics, and influence of m on the band gap and the thermal conductivity. *Journal of the American Ceramic Society*, 2020, **103**(5), P. 3030–3038.
- [4] Zhang C., Pei Y., Zhao L.-D., Berardan D., Dragoe N., Gong S., Guo H., The phase stability and thermophysical properties of $\text{InFeO}_3(\text{ZnO})_m$ ($m = 2, 3, 4, 5$). *Journal of the European Ceramic Society*, 2014, **34**(1), P. 63–68.
- [5] Katayose S., Miyazaki T., Hayashi Y., Takizawa H. Synthesis of natural superlattice structure in the binary $\text{ZnO}-\text{Fe}_2\text{O}_3$ system by microwave irradiation. *Journal of the Ceramic Society of Japan*, 2010, **118**(1377), P. 387–389.
- [6] Kimizuka N., Yamazaki S. *Physics and Technology of Crystalline Oxide Semiconductor CAAC-IGZO: Fundamentals (Wiley Series in Display Technology)*. John Wiley & Sons, Ltd., 2016, 352 p.
- [7] Costa J.C., Pouryazdan A., Panidi J., Spina F., Anthopoulos T.D., Liedke M.O., Schneider C., Wagner A., Münzenrieder N. Flexible IGZO TFTs and their suitability for space applications. *IEEE Journal of the Electron Devices Society*, 2019, **7**, P. 1182–1190.
- [8] InGaZnO (IGZO) System For Gas Detection at Room Temperature. United States Patent US 20220365022 A1. United States Patent and Trademark Office. Vijjapu M.T., 11 p.
- [9] Kimizuka N., Isobe M., Nakamura M., Mohri T. Syntheses and crystallographic data of the homologous compounds $\text{InFeO}_3(\text{ZnO})_m$ ($m = 1, 2, 3, 7, 11, 13, 15$, and 19) and $\text{Fe}_2\text{O}_3(\text{ZnO})_m$ ($m = 8$ and 9) in the $\text{In}_2\text{O}_3-\text{ZnFe}_2\text{O}_4-\text{ZnO}$ system. *Journal of Solid State Chemistry*, 1993, **103**(2), P. 394–402.
- [10] Qu W.-W., Zhang X.-X., Yuan B.-F., Zhao L.-D. Homologous layered $\text{InFeO}_3(\text{ZnO})_m$: new promising abradable seal coating materials. *Rare Metals*, 2018, **37**, P. 79–94.
- [11] Wu J., Wei X., Pature N.P., Klemens P.G., Gell M., Garcia E., Miranzo P., Osendi M.I. Low-thermal-conductivity rare-earth zirconates for potential thermal-barrier-coating applications. *Journal of the American Ceramic Society*, 2002, **85**(12), P. 3031–3035.
- [12] Zhao L.-D., Pei Y.-L., Liu Y., Berardan D., Dragoe N. InFeZnO_4 as promising thermal barrier coatings. *Journal of the American Ceramic Society*, 2011, **94**(6), P. 1664–1666.
- [13] Pan W., Phillpot S.R., Wan C., Chernatynskiy A., Qu Z. Low thermal conductivity oxides. *MRS Bulletin*, 2012, **37**, P. 917–922.
- [14] Guo H., Zhang C., Pei Y., Guo L., Gong S. Improved thermal barrier properties of InFeZnO_4 ceramics by Gd/Yb doping. *Journal of Alloys and Compounds*, 2014, **585**, P. 404–406.
- [15] Zhang L., Pei Y., Guo H., Gong S. Thermal transport properties of $\text{InFeZnO}_4-\text{YbFeZnO}_4$ solid solutions. *Journal of Alloys and Compounds*, 2015, **623**, P. 203–208.
- [16] Zhao B., Pei Y., Zhang L., Gong S., Zhao L.-D. Thermal and mechanical properties of Yb&Mg co-doped InFeZnO_4 . *Journal of Alloys and Compounds*, 2016, **684**, P. 34–39.
- [17] Zinkle S.J. Hardness and depth-dependent microstructure of ion-irradiated magnesium aluminate spinel. *Journal of the American Ceramic Society*, 1989, **72**(8), P. 1343–1351.
- [18] Fukushima Y., Yano T., Maruyama T. Swelling, thermal diffusivity and microstructural investigation of neutron irradiated single crystals of nonstoichiometric spinel. *Journal of Nuclear Materials*, 1990, **175**(3), P. 203–208.
- [19] Kimizuka N., Mohri T., Matsui Y. Homologous Compounds, $\text{InFeO}_3(\text{ZnO})_m$ ($m = 1-9$). *Journal of Solid State Chemistry*, 1988, **74**(1), P. 98–109.
- [20] Narendranath S.B., Kumar Yadav A., Bhattacharyya D., Nath Jha S., Nandini Devi R. Photocatalytic H_2 evolution from water-methanol system by anisotropic $\text{InFeO}_3(\text{ZnO})_m$ oxides without cocatalyst in visible light. *ACS Applied Materials & Interfaces*, 2014, **6**(15), P. 12321–12327.
- [21] Smirnova M.N., Kondrat'eva O.N., Nikiforova G.E., Khoroshilov A.V. A new approach to prepare LuFeMgO_4 . *Russian Journal of Inorganic Chemistry*, 2023, **68**, P. 507–514.
- [22] Smirnova M.N., Kondrat'eva O.N., Nikiforova G.E., Yapryntsev A.D., Averin A.A., Khoroshilov A.V. Features of synthesis of InGaMgO_4 from nitrate-organic precursors and study of its physical properties. *Russian Journal of Inorganic Chemistry*, 2024, (in press).
- [23] Larkin P.J. *Infrared and Raman Spectroscopy: Principles and Spectral Interpretation*. Elsevier, 2011, 230 p.
- [24] Jain D., Sudarsan V., Patra A.K., Sastry P.U., Tyagi A.K. Effect of local ordering around Th^{4+} ions in glycine-nitrate precursor gel on the powder characteristic of gel-combusted ThO_2 . *Journal of Nuclear Materials*, 2019, **527**, P. 151826.
- [25] Warriar A.V.R., Narayanan P.S. Infrared absorption spectra of single crystals of glycine silver nitrate and monoglycine nitrate. *Proceedings of the Indian Academy of Sciences – Section A*. 1967, **66**, P. 46–54.
- [26] Khrushchev M.M. *Trenie, iznos i mikrotverdost' materialov: Izbrannye raboty (k 120-letiyu so dnya rozhdeniya)*. KRASAND, Moskva, 2012, 512 p.
- [27] Lebedeva S.I. *Opredelenie mikrotverdosti mineralov*. Izdatel'stvo akademii nauk SSSR, Moskva, 1963, 124 p.
- [28] Andrade P.H.M., Volkringer C., Loiseau T., Tejeda A., Hureau M., Moissette A. Band gap analysis in MOF materials: Distinguishing direct and indirect transitions using UV-vis spectroscopy. *Applied Materials Today*. 2024, **37**, P. 102094.
- [29] Meng X., Wang Z., Qiu K., Li Y., Liu J., Wang Z., Liu S., Li X., Yang Z., Li P. Design of a novel near-infrared phosphor by controlling cationic coordination environment. *Crystal Growth & Design*, 2018, **18**(8), P. 4691–4700.
- [30] Naguib H.M., Kelly R. Criteria for bombardment-induced structural changes in non-metallic solids. *Radiation Effects*, 1975, **25** (1), P. 1–12.
- [31] Batsanov S.S. The concept of electronegativity. Conclusions and prospects. *Russian Chemical Reviews*, 1968, **37**(5), P. 332–351.
- [32] Satalkar M., Kane S.N., Kulriya P.K., Avasthi D.K. Swift heavy ion irradiated spinel ferrite: A cheap radiation resistant material. *Nuclear Instruments and Methods in Physics Research Section B: Beam Interactions with Materials and Atoms*, 2016, **379**, P. 235–241.
- [33] Studer F., Houpert Ch., Groult D., Yun Fan J., Meftah A., Toulemonde M. Spontaneous magnetization induced in the spinel ZnFe_2O_4 by heavy ion irradiation in the electronic stopping power regime. *Nuclear Instruments and Methods in Physics Research Section B: Beam Interactions with Materials and Atoms*, 1993, **82**(1), P. 91–102.

Submitted 11 October 2024; accepted 15 October 2024

Information about the authors:

Olga N. Kondrat'eva – Kurnakov Institute of General and Inorganic Chemistry of the Russian Academy of Sciences, Leninskii prosp., 31, Moscow, 119991, Russia; ORCID 0000-0003-2508-9868; ol.kondratieva@gmail.com

Maria N. Smirnova – Kurnakov Institute of General and Inorganic Chemistry of the Russian Academy of Sciences, Leninskii prosp., 31, Moscow, 119991, Russia; ORCID 0000-0003-2707-7975; smirnovamn@igic.ras.ru

Galina E. Nikiforova – Kurnakov Institute of General and Inorganic Chemistry of the Russian Academy of Sciences, Leninskii prosp., 31, Moscow, 119991, Russia; ORCID 0000-0002-2892-6054; gen@igic.ras.ru

Alexey D. Yaprntsev – Kurnakov Institute of General and Inorganic Chemistry of the Russian Academy of Sciences, Leninskii prosp., 31, Moscow, 119991, Russia; ORCID 0000-0001-8166-2476; yaprntsev@igic.ras.ru

Dmitriy F. Kondakov – Kurnakov Institute of General and Inorganic Chemistry of the Russian Academy of Sciences, Leninskii prosp., 31, Moscow, 119991, Russia; ORCID 0000-0001-8636-5462; oldradio@mail.ru

Leonid D. Yagudin – Frumkin Institute of Physical Chemistry and Electrochemistry of the Russian Academy of Sciences Leninskii prosp., 31.4, Moscow, 119071, Russia; yagudinld@icloud.com

Conflict of interest: the authors declare no conflict of interest.